Determination of tilt angle and its behavior in chiral smectic phases by exploring molecular conformations using complementary methods

A. Deptuch,[1,*] T. Jaworska-Gołąb,[2] M. Dziurka,[3] J. Hooper,[3] M. Srebro-Hooper,[3] M. Urbańska,[4] M. Tykarska,[4] and M. Marzec[2]

[1]*Institute of Nuclear Physics Polish Academy of Sciences, Radzikowskiego 152, PL-31342 Kraków, Poland*
[2]*M. Smoluchowski Institute of Physics, Jagiellonian University, Łojasiewicza 11, PL-30348 Kraków, Poland*
[3]*Faculty of Chemisty, Jagiellonian University, Gronostajowa 2, PL-30387 Kraków, Poland*
[4]*Institute of Chemistry, Military University of Technology, Kaliskiego 2, PL-00908 Warsaw, Poland*

(Received 27 October 2022; accepted 21 February 2023; published 17 March 2023)

Density functional theory (DFT) calculations and x-ray diffraction techniques were employed to evaluate the value of the tilt angle in ferroelectric smectic C^* and antiferroelectric smectic C_A^* phases. Five homologues from the chiral series denoted as 3FmHPhF6 ($m = 2, 4, 5, 6, 7$), based on 4-(1-methylheptyloxycarbonyl) phenyl 4'-octyloxybiphenyl-4-carboxylate (MHPOBC), were studied. Two types of conformations for the nonchiral terminal chain (fully extended and *gauche*) and three types of deviation from the rodlike shape of the molecules (hockey stick, zigzag, and C shape) were computationally considered. The nonlinear shape of the molecules was accounted for by introducing a shape parameter $\delta\Theta$. We observe that calculations of the tilt angle which consider the C-shaped structures, in both the fully extended or *gauche* conformations, lead to good agreement with the values of the tilt angle obtained from electro-optical measurements below the saturation temperature. The results allow us to conclude that such structures are adopted by molecules in the examined series of smectogens. Additionally, this study proves the presence of the standard orthogonal SmA^* phase for the homologues with $m = 6, 7$, and the de Vries SmA^* phase for $m = 5$.

DOI: 10.1103/PhysRevE.107.034703

I. INTRODUCTION

Smectic liquid crystals, which are phases where the molecules are arranged into layers [1–4], are objects of study due to their potential use in liquid crystal displays (LCDs) [2,3], LC-based colloids [4], organic electronics [4,5] and anisotropic glasses with various order [5,6]. The first field, LCDs, is currently dominated by nematic liquid crystals, but it is known that the chiral tilted smectic phases are also suitable for this application, especially the orthoconic antiferroelectric one [2,3]. The ferroelectric smectic C^* phase (SmC^*) shows a quasi-long-range layer order in one dimension, with a synclinic order of molecular tilt angles in neighboring layers [Fig 1(a)]. The antiferroelectric smectic C_A^* phase (SmC_A^*) differs from SmC^* because it has an anticlinic ordering of the tilt angle in neighboring layers [Fig. 1(b)]. The positional order within the smectic layers of both phases (SmC^* and SmC_A^*) is only short range, the same as in liquids. The molecules' chirality lowers the symmetry of the phase (compared to an achiral tilted smectic phase) and allows for a nonzero polarization of a smectic layer in a direction perpendicular to the tilt plane, which occurs if the molecules possess a nonzero dipole moment in this direction [1–3]. Another common feature of the chiral tilted smectic phases is a helicoidal order in the direction perpendicular to the smectic layer plane, which overlaps with the synclinic or anticlinic ordering of the tilt angle. The pitch of the helix is much larger than the smectic layer spacing [1–3]. The presence of the helical order averages the spontaneous polarization of the bulk to zero, therefore the switching of molecules by an external electric field is possible only after unwinding the helix, e.g., by proper boundary conditions [2,3,7,8].

The chiral smectic-based LCDs work via the Clark-Lagerwall effect [7], which is also the basis of the electro-optic method for tilt angle determination. The Clark-Lagerwall effect can be observed for a planar aligned sample (bookshelf geometry) in an electro-optic cell, and within such a setup the switching of molecules occurs within the tilt plane [Fig. 1(c)]. The electric field causes switching of molecules only above a certain threshold value [1–3]. If the pertinent conditions are fulfilled, a bistable switching between two ferroelectric states (for two antiparallel orientations of the external field $\vec{E}$) is observed for the SmC^* phase [7]. For the SmC_A^* phase there are three states: two ferroelectric ones for two orientations of $\vec{E}$ and an antiferroelectric state for a zero field [8]. The tilt angle Θ can be determined by rotating the sample and observing its texture under a polarizing optical microscope (POM); such an angle that is measured directly by the electro-optic method is referred to as the optical tilt angle Θ_{POM}. The total extinction of transmitted light occurs when the direction of the tilt overlaps with the direction of the axis of one of the polarizers [Fig. 1(d)]. When the external electric field is switched to an opposite direction, the same happens with the transverse dipole moments of molecules (dipole moments perpendicular to the tilt plane), causing them

*aleksandra.deptuch@ifj.edu.pl

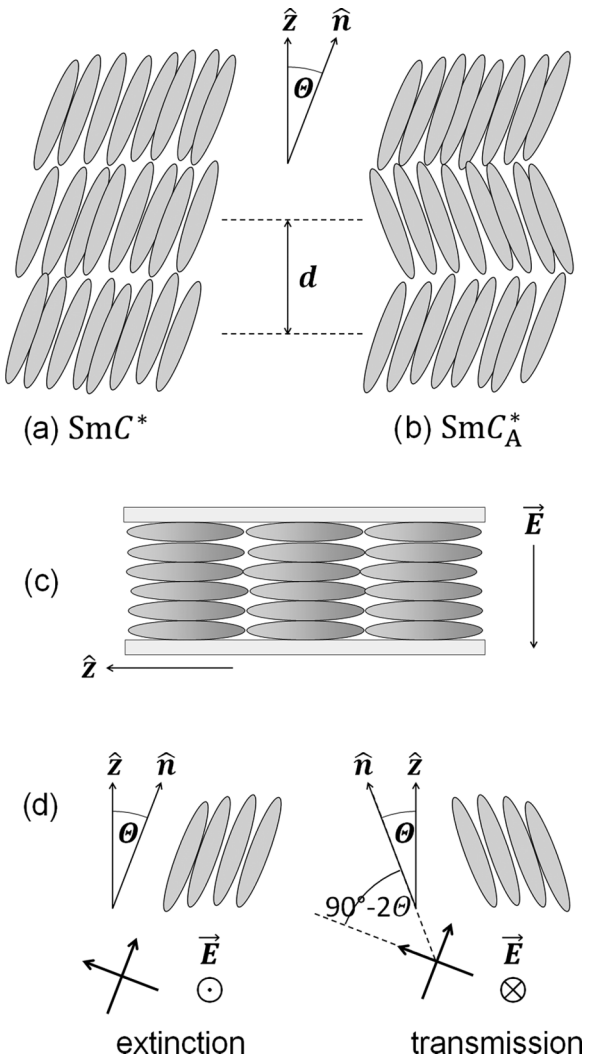

FIG. 1. Ordering of molecules in the ferroelectric SmC^* (a) and antiferroelectric SmC_A^* (b) phases along with a side view of an electro-optic cell with a smectic phase in a bookshelf geometry (c) and switching of the molecules by an electric field (d). Perpendicular arrows in the bottom of (d) visualize the optic axes of the polarizers. Vector $\hat{z}$ is the smectic layer's normal, $\hat{n}$ is the director, $\vec{E}$ denotes the external electric field, Θ is the tilt angle, and d is the smectic layer spacing. Both $\hat{z}$ and $\hat{n}$ vectors lay in the tilt plane, parallel to the plane of the electro-optic cell.

to rotate around the layer's normal. The transmission of the light is now >0 and in order to obtain the total extinction, the sample needs to be rotated by 2Θ or $90^\circ - 2\Theta$. The special case is the orthoconic smectic phase with $\Theta = 45^\circ$, wherein total extinction is observed for both orientations of the electric field for the same angular position of the sample [9].

In LCDs based on the antiferroelectric SmC_A^* phase, the optical axes of the polarizers are mutually parallel and perpendicular to the axis $\hat{z}$ of the tilt cone; therefore the total extinction is expected for a zero external field when the sample is in the antiferroelectric state [2,3,9]. For $\Theta = 45^\circ$ the smectic phase becomes optically uniaxial and its optical axis is perpendicular to the tilt plane and electro-optic cell plane. This considerably diminishes the problem of alignment defects which can cause nonzero transmission in the dark state. The tilt angle $\Theta = 45^\circ$ also maximizes the transmission of light in the ferroelectric states, as in this setup the tilt direction is exactly between the polarizers' axes [9]. This is why one of the main aims of investigating chiral smectic phases is to search for compounds which exhibit the orthoconic SmC_A^* phase.

The electro-optic method is not the only way to determine the tilt angle in the smectic phases. The smectic layer spacing d, which is a structural parameter connected with the tilt angle, can be assessed using the x-ray diffraction (XRD) method. If one obtains the value of the molecular length l, either from the molecular modeling or from the smectic layer spacing in the orthogonal ($\Theta = 0$) paraelectric SmA^* phase, it is possible to calculate the tilt angle as $\Theta_{\mathrm{XRD}} = \arccos(d/l)$. The Θ_{XRD} value obtained this way is referred to as the steric tilt angle [10,11]. Due to the size of typical mesogens, theoretical calculations are usually performed for isolated molecules, especially when the structure of the crystal phase is unknown. Because of this, it is difficult to take into account intermolecular interactions that can influence the actual shape of molecules packed within smectic layers. On the other hand, when the molecular length is taken as equal to the layer spacing in the SmA^* phase, it can be underestimated because of the interdigitation of neighboring smectic layers [12]. Additionally, the SmA^* phase may turn out to be of the de Vries type, which means that despite the fact that the average tilt angle is zero, particular molecules are tilted in random directions [12,13]. The presence of the de Vries phase may also lead to underestimation of the molecular length.

There is a known discrepancy between the values of the tilt angle measured directly by the electro-optic method (Θ_{POM}) and the steric tilt angle (Θ_{XRD}) that is obtained from the d/l ratio. The optical tilt angle has usually higher values than the steric tilt angle [10,11,14–19] but there are also cases where the steric tilt angle is larger [10,20]. The differences between Θ values determined by these two methods are generally explained by the structure of molecules that form chiral smectic phases, comprising an aromatic rigid core and two flexible terminal chains (based on the structure of the first antiferroelectric liquid crystal 4-(1-methylheptyloxycarbonyl) phenyl 4'-octyloxybiphenyl-4-carboxylate, abbreviated as MHPOBC [8]). Such molecular structure allows for various conformations that can differ from the rodlike one, for example, the hockey-stick, zigzag, or C-shaped conformations [Fig. 2(b)] [10,14,20–22]. This means that the tilt of the rigid cores of molecules can be different than that of the whole molecule [10,11,16–18,20]. Other sources of this discrepancy can be the mentioned interdigitation of smectic layers or even the formation of dimers [17].

The homologous series of (*S*)-4′-(1-methylheptyloxycarbonyl) biphenyl-4-yl 4-[7-(2,2,3,3,4,4,4-heptafluorobutoxy)alkyl-1-oxy]-2-fluorobenzoates with a C_mH_{2m} carbon chain [abbreviated as 3FmHPhF6, Fig. 2(a)] is a series of liquid crystalline compounds which exhibit the ferroelectric SmC^* and/or antiferroelectric SmC_A^* phases over a wide temperature range [22–25]. For the higher homologues, with $m \geqslant 5$, the presence of the paraelectric SmA^* phase [22–25] and the glass transition from the SmC_A^*

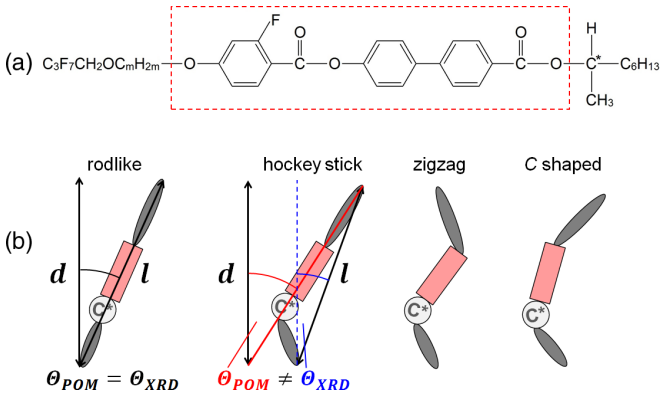

FIG. 2. Molecular formula of the 3FmHPhF6 series (a) and schematic representation of exemplary conformations possible for a molecule with a rigid core and two terminal chains (b). The dashed frame in (a) indicates the molecular core which was used in calculations of the shape parameter $\delta\Theta$ (details in the text). In (b), d is the smectic layer spacing, l is the molecular length, and Θ_{POM} and Θ_{XRD} are the optical and steric tilt angle, respectively.

phase [22,25] were reported. The largest tilt angle in the SmC_A^* phase of the 3FmHPhF6 homologues and its mixtures with similar compounds, measured by the electro-optic method, is $\Theta_{\mathrm{POM}} = 40°$–$45°$ [24–27].

In 2017, we presented the use of molecular modeling and x-ray diffraction for determination of the tilt angle in the SmC^* and SmC_A^* phases of the 3F7HPhF6 compound, as the electro-optic method could not be applied due to difficulties with the sample alignment [22]. We proposed introducing a shape parameter, denoted as $\delta\Theta$, which corresponds to the difference between the orientation of the whole molecule and that of the molecular core. Such a parameter allows us to account for the nonlinear shape of the molecule in the calculations of the tilt angle via the following formula:

$$\Theta = \Theta_{\mathrm{XRD}} + \delta\Theta = \arccos(d/l) + \delta\Theta. \quad (1)$$

For 3F7HPhF6, the hockey-stick shape of molecules and maximally extended conformation were assumed. The tilt angle determined from Eq. (1) was $\Theta = 45.0(4)°$ below the saturation temperature, including the shape parameter $\delta\Theta = 7.5°$; however, this result was based only on one molecular conformation (the extended, hockey-stick one) [22].

Herein, we present determination of the steric tilt angle in the SmC^* and SmC_A^* phases for the series of 3FmHPhF6 homologues with $m = 2$, 4, 5, 6, 7; this includes using the smectic layer spacing that is determined from x-ray diffraction patterns and also more detailed structural characteristics of molecular models optimized with density functional theory (DFT) calculations. In order to evaluate the molecular length and shape in a more reliable way, several conformations of molecules are considered, including four extended *max* conformations, used by us previously to estimate dipole moments [25], and also models with *gauche* conformations of O-C and/or C-C bonds in the nonchiral $C_3F_7CH_2OC_mH_{2m}O$– chain. The results are compared with the corresponding optical tilt angle values [25,26] in order to determine which conformation(s) of molecules within the smectic layers is (are) the most probable. The differences in the structure of the paraelectric SmA^* phase for homologues with $m = 5$, 6, 7 are also discussed in relation to the presence of the de Vries phase.

II. EXPERIMENTAL AND COMPUTATIONAL DETAILS

Smectic phases of the (*S*)-4′-(1-methylheptyloxycarbonyl) biphenyl-4-yl 4-[7-(2,2,3,3,4,4,4-heptafluorobutoxy)alkyl-1-oxy]-2-fluorobenzoates series with a C_mH_{2m} carbon chain ($m = 2$, 4–7) were studied. The samples were synthesized as described in Refs. [23,24].

A. X-ray diffraction

Low-angle XRD measurements ($2\theta \approx 2°$–$3.5°$) of the smectic layer spacing were carried out on flat samples deposited on a Si wafer (D8 Discover, Bruker; Anton Paar DC350 nonambient attachment, Cu $K\alpha$). They were performed on cooling from the isotropic liquid phase (100 °C–110 °C) down to 30 °C at each 1 °C. For homologues with $m = 5$, 6, and 7, additional measurements in the vicinity of the Sm$A^* \rightarrow$ SmC^* transition were also done at each 0.1 °C on cooling. Complementary wide-angle measurement for $m = 7$ at 80 °C was carried out for a sample in the form of a droplet on the metallic stage (D8 GADDS, Bruker; Cu $K\alpha$, $2\theta = 1°$–$30°$). It allowed us to determine the value of the smectic layer spacing from the first and second order diffraction peaks and correct the systematic shift of ca. 0.5 Å observed between the results of two low-angle measurements published in [22].

B. Molecular modeling

Quantum-mechanical calculations for isolated molecules in 20 different conformations (for details see Sec. III A and Ref. [25]) were performed. Starting models were optimized either with the semiempirical AM1 method [28] in GAUSSIAN09 [29] or by the PM7 method [30] in MOPAC2016 [31], and then reoptimized with the DFT method in GAUSSIAN09. The BLYP [32,33] exchange-correlation functional and the third-generation Grimme's set of semiempirical dispersion corrections D3 with Becke-Johnson damping [34] were employed in the DFT calculations along with the SVP basis set [35–37]. The results were visualized and analyzed in AVOGADRO [38].

III. RESULTS AND DISCUSSION

A. Molecular modeling

The geometries of individual (isolated) molecules were initially optimized in maximally extended conformations, leading to the four *max* geometries that are shown in Fig. 3(a) for 3F5HPhF6: this set includes two geometries with a hockey-stick shape (*max*1 and *max*4), one with a C shape (*max*2), and one with a zigzag shape (*max*3). Note that genuinely rodlike molecules were not obtained. The considered *max* conformations, selected to represent different relative orientations of the $C_3F_7CH_2OC_mH_{2m}O$– and –COOC*$HCH_3C_6H_{13}$ chains within each system, correspond to the local minima in conformational energy scans over two torsional angles, namely, –C–O–C–C– between the nonchiral

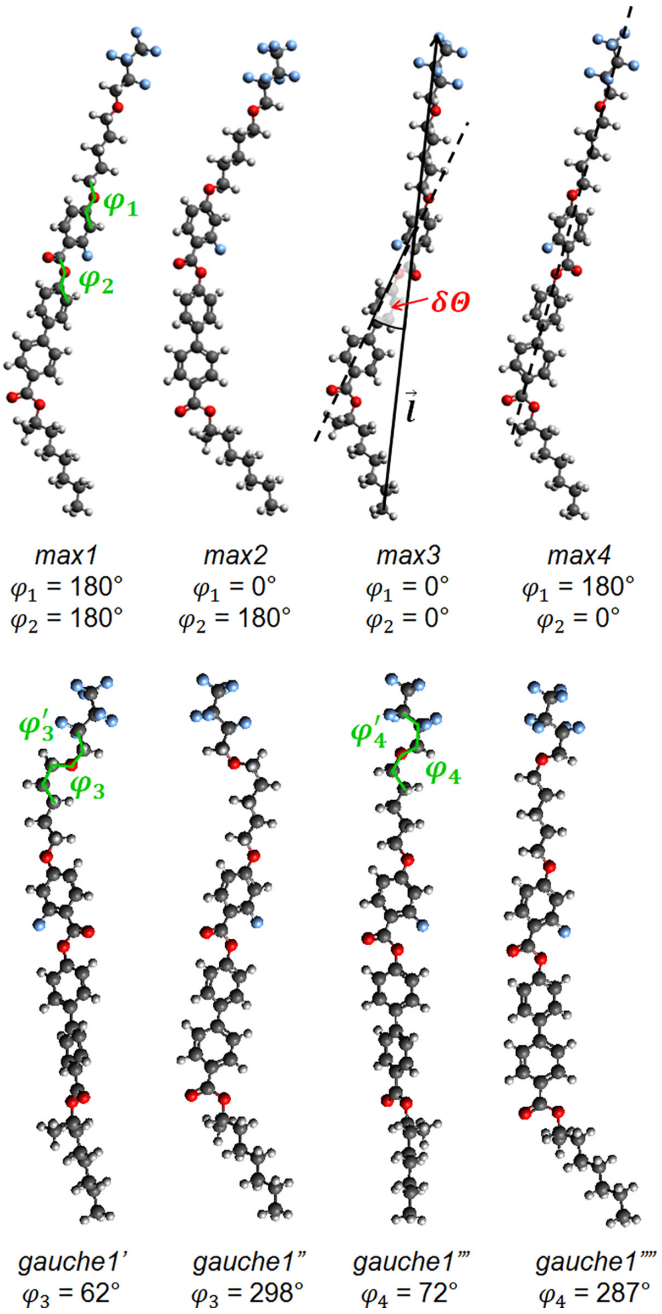

FIG. 3. Visualization of the considered conformations for the 3F5HPhF6 molecule optimized with DFT-BLYP/SVP, representative for the remaining 3F*m*HPhF6 homologues. The upper row shows four extended *max* conformations. The bottom row shows four representative *gauche* conformations obtained from *max*1. Definition of the shape parameter $\delta\Theta$ is presented for *max*3.

chain and benzene ring, denoted as φ_1 (Fig. 3), and –C–O–C–C– between the benzene ring and biphenyl, denoted as φ_2. The conformational transitions of *max*1 → *max*2 or *max*4 → *max*3 require the change of the φ_1 angle from 180° to 0° and have an energy barrier of at least 20 kJ/mol, as assessed by DFT-BLYP/SVP calculations for $m = 5$ [Fig. 4(a)]. Meanwhile, the *max*1 → *max*4 and *max*2 → *max*3 transformations occur by the change of the φ_2 angle from 180° to 0°, and they have a much smaller energy barrier of ca. 5 kJ/mol

TABLE I. Potential energy values in kJ/mol computed with DFT-BLYP/SVP for isolated 3F*m*HPhF6 molecules ($m = 2, 4, 5, 6, 7$) in various conformations. The energies for each compound are given relative to the lowest-energy conformations, which are *gauche*3′ and *gauche*3″ for all homologues (highlighted in bold).

	m				
Conformation	2	4	5	6	7
*max*1	10.4	11.5	12.1	11.4	11.3
*gauche*1′	1.3	1.3	1.3	1.3	1.3
*gauche*1″	1.2	1.3	1.3	1.3	1.3
*gauche*1‴	6.2	10.6	10.7	10.1	9.8
*gauche*1⁗	6.1	10.6	10.8	10.1	9.8
*max*2	9.4	10.4	10.9	10.2	10.1
*gauche*2′	0.1	0.1	0.1	0.1	0.1
*gauche*2″	0.1	0.1	0.1	0.1	0.1
*gauche*2‴	5.1	9.5	9.6	8.9	8.6
*gauche*2⁗	5.1	9.5	9.6	8.9	8.6
*max*3	9.3	10.3	10.8	10.1	10.0
***gauche*3′**	**0.0**	**0.0**	**0.0**	**0.0**	**0.0**
***gauche*3″**	**0.0**	**0.0**	**0.0**	**0.0**	**0.0**
*gauche*3‴	5.0	9.4	9.5	8.8	8.5
*gauche*3⁗	5.0	9.4	9.5	8.8	8.5
*max*4	10.4	11.5	12.1	11.3	11.3
*gauche*4′	1.2	1.3	1.3	1.2	1.3
*gauche*4″	1.1	1.2	1.2	1.2	1.2
*gauche*4‴	6.1	10.6	10.7	10.0	9.7
*gauche*4⁗	6.1	10.6	10.7	10.0	9.7

[Fig. 4(b)]. The differences between the local minima of *max*1, *max*2, *max*3, and *max*4, on the considered DFT potential energy surface, are ca. 1 kJ/mol (Table I). In the studied series of mesogens, molecules are relatively closely packed within the smectic layers, as the average intralayer distances do not exceed 4.9 Å, which is comparable with the width of the aromatic core of a molecule obtained from DFT calculations (4.3–4.5 Å) [22,25]. One should notice that molecules in the hockey-stick, C-shaped, and zigzag conformations are not exactly compatible with each other in terms of the supposed close packing within the smectic layers; therefore we assume that all molecules in the layer should adopt a rather similar shape. This means that the *max*1 and *max*4 conformations, both hockey stick, can be analyzed together within the set of conformations denoted as *max*1 + 4, while *max*2 and *max*3 conformations should be analyzed separately.

It is, however, reasonable to assume that not all molecules adopt the "maximally extended" conformations that come about from all C-C and C-O bonds in the terminal chains being in antiperiplanar conformations, as it is in the *max* models. Two types of a *gauche* conformation were accordingly constructed by modifying torsional angles in the $–CH_2OC_mH_{2m}O–$ chain (Fig. 3): the $—O–C_m–C_{m-1}–C_{m-2}–$ angle (for $m = 2$, –O–C–C–O–), denoted as φ_3, and the $–C–O–C_m–C_{m-1}–$ angle, denoted as φ_4. In order to preserve the molecular shape obtained for the *max* conformations, twisting of the φ_3, φ_4 angles in the starting models was performed along with simultaneous opposite twisting of the $\varphi'_3 = -\varphi_3$, $\varphi'_4 = -\varphi_4$ angles, which effectively adds concerted

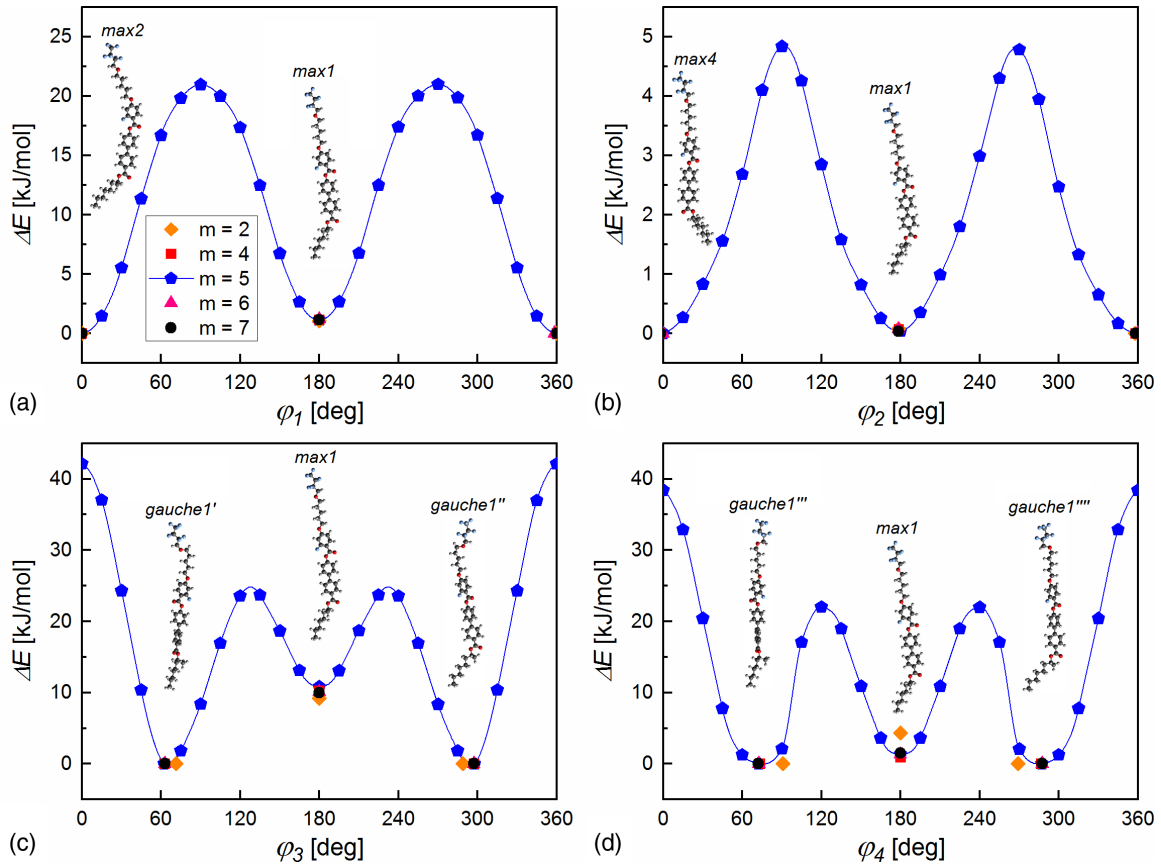

FIG. 4. Potential energy profiles for rotational scans performed for the isolated 3F5HPhF6 molecule with the DFT-BLYP/SVP method. In each panel, ΔE is given relative to the most energetically favorable conformation. The φ_1, φ_2, φ_3, φ_4 torsional angles are defined in the main text and in Fig. 3. For other investigated 3FmHPhF6 compounds, DFT geometry optimizations were performed only for the local minima analogous to those identified for 3F5HPhF6.

sets of rotations around the next-nearest-neighbor bonds, i.e., –CF_2–CH_2–O–CH_2– and –CF_2–CF_2–CH_2–O–, respectively. The conformational energy scans [Figs. 4(c) and 4(d)] show two local energy minima for each type of the *gauche* conformation, with $\varphi_3 \approx 60^\circ$ or 300° (labeled as *gauche*′ and *gauche*″, respectively) and $\varphi_4 \approx 70^\circ$ or 290° (*gauche*‴ and *gauche*⁗) for $m = 4$–7. For $m = 2$, the local minima were obtained for $\varphi_3 \approx 70^\circ$ or 290° and $\varphi_4 \approx 90^\circ$ or 270°, due to the proximity of oxygen atoms. The *gauche* conformations are more energetically favorable than their parent *max* models with φ_3 and $\varphi_4 \sim 180^\circ$, because they introduce more noncovalent intramolecular –C–H . . . F–C– and –C–H . . . [−]O– contacts along the chains. As computed for 3F5HPhF6, the energy barrier for the *max* → *gauche* transformation is 13 and 21 kJ/mol for the φ_3 and φ_4 angle, respectively. As summarized in Table I, for all homologues, the lowest-energy conformations among all of the conformations considered here are those of the type *gauche*′ and *gauche*″. The potential energy of *gauche*‴ and *gauche*⁗ is higher than that of *gauche*′ and *gauche*″ by ca. 5 kJ/mol for $m = 2$ and ca. 9 kJ/mol for $m = 4$–7, and the potential energy of *max* conformations is higher than that of *gauche*‴ and *gauche*⁗ by ca. 5 kJ/mol for $m = 2$ and ca. 1 kJ/mol for $m = 4$–7. The difference between $m = 2$ and longer homologues is caused by proximity of two oxygen atoms in the nonchiral chain of the 3F2HPhF6 molecule, which modifies the potential energy landscape compared to $m = 4$–7. Nevertheless, the resulting energetic order of the examined structures appears to be independent of m and follows the trend: *gauche*′ and *gauche*″ < *gauche*‴ and *gauche*⁗ < *max*, with the zigzag-shaped (*3*) and C-shaped (*2*) conformations exhibiting lower DFT energies than the hockey-stick-shaped (*4* and *1*) ones.

Because the RT value (R is the universal gas constant) for $T = 80$ °C is equal to ca. 3 kJ/mol, the considered conformations are not equally probable even at this temperature. This means that the average value of any observable A discussed in the following should be calculated as the Boltzmann average:

$$\langle A \rangle = \frac{\sum_{\text{conf}} A_j \exp\left(-\frac{\Delta E_j}{k_B T}\right)}{\sum_{\text{conf}} \exp\left(-\frac{\Delta E_j}{k_B T}\right)}, \tag{2}$$

where Σ_{conf} is the summation over all considered conformations, A_j is the observable value obtained for the jth conformation, and ΔE_j is the energy of the jth conformation with respect to the lowest-energy one.

Let us first define and analyze the molecular length and shape parameter for the considered 3FmHPhF6 structures. In the following, the molecular length l is the length of the vector connecting the last carbon atom in the chiral terminal chain and the most distant fluorine atom on the other end

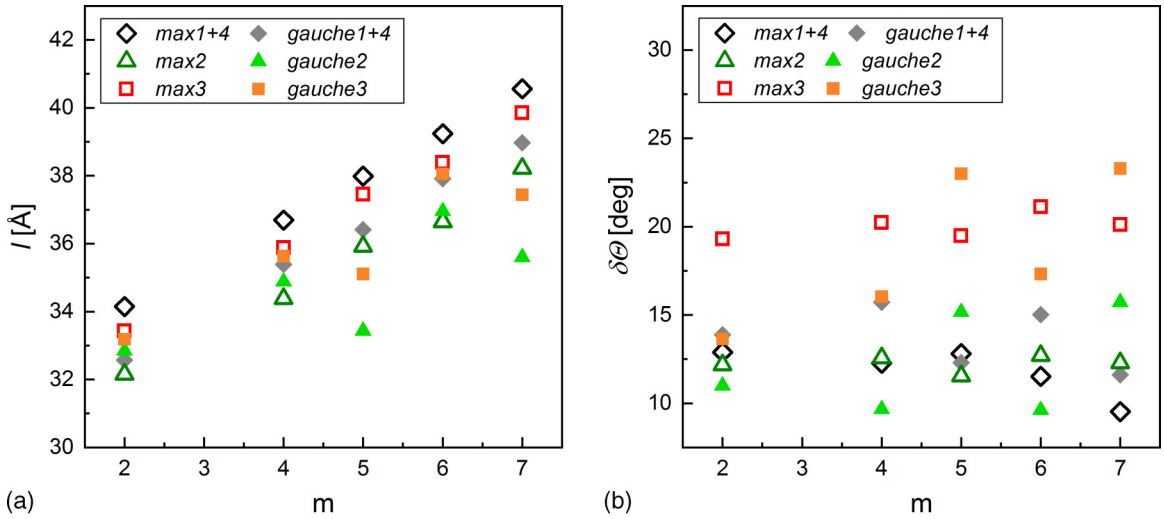

FIG. 5. Boltzmann-averaged values of the molecular length (a) and the shape parameter (b) calculated for 3F*m*HPhF6 molecules at 80 °C in *max* and *gauche* conformations, separately for the hockey-stick shape (1 + 4), C shape (2), and zigzag shape (3).

of the 3F*m*HPhF6 molecule (Fig. 3). Figure 5(a) shows the l values calculated as the Boltzmann averages at 80 °C (this is chosen as a representative temperature; the Boltzmann averages do not depend strongly on temperature in the stability range of the SmC^* and SmC_A^* phases) over *max* conformations with the same shape (*max*1 + 4—two conformations, *max*2, *max*3) and over *gauche* conformations derived from each *max* set (*gauche*1 + 4—eight conformations; *gauche*2—four conformations; *gauche*3—four conformations). The Boltzmann averages including both corresponding *max* and *gauche* conformations are not shown because they are almost equal to results obtained by averaging over the *gauche* structures only, due to the lower energies of the *gauche* conformers (Table I). The molecular length in most cases increases with increasing m; it was found that the differences in the calculated l values do not exceed 5 Å for different conformers of the same compound. The largest l values are obtained for *max*1 + 4, while slightly smaller ones are seen for *max*3, and the smallest for *max*2; the average molecular length for the *gauche* conformations is generally between those obtained for *max*3 and *max*2, except for the *gauche*2 and *gauche*3 structures of the odd homologues with $m = 5, 7$, for which a substantial decrease in l is visible.

The definition of the shape parameter $\delta\Theta$ was based on the orientation of the region with the aromatic core, as highlighted by the dashed frame in Fig. 2(a). The vector describing an average orientation of atoms within this fragment was calculated by means of linear regression and the $\delta\Theta$ value was computed as the angle between this vector and the $\vec{l}$ vector, which is visualized in Fig. 3 for the *max*3 conformation. After computing $\delta\Theta$ in such a fashion for every conformation, the Boltzmann-averaged shape parameter values that were computed for 3F*m*HPhF6 in all of the different conformations are compared in Fig. 5(b). The $\delta\Theta$ values calculated for the *max*1 + 4, *gauche*1 + 4, *max*2, and *gauche*2 sets of particular homologues are within the 9.5°–15.7° range, and they are generally smaller than the $\delta\Theta$ values obtained for the corresponding *max*3 and *gauche*3 sets, which are in the 13.6°–23.3° range. Only for $m = 2$ is the $\delta\Theta$ value for the *gauche*1 + 4 set slightly larger than that for *gauche*3. The odd-even effect is more pronounced for the *gauche* sets than for their *max* counterparts.

B. Smectic layer spacing

The temperature dependence of the smectic layer spacing d, determined from the diffraction patterns collected at each 1 °C upon cooling, is presented in Fig. 6(a). The d values decrease with decreasing temperature and stabilize below ca. 60 °C. The asymptotic value, reached well in the SmC_A^* phase for all compounds, increases linearly with increasing m (by ∼ 0.8 Å for each –CH_2– group added to the –C_mH_{2m}– chain), which means that similar packing of molecules for all studied homologues can be expected [39]. The SmC^* → SmC_A^* transition reveals itself as a step in the temperature dependence of d [marked by dashed lines in Fig. 6; see also inset in Fig. 6(a)]. The largest observed layer spacing for $m = 5, 6, 7$ was interpreted as the one characterizing the paraelectric SmA^* phase. Since the SmA^* phase of these homologues is present only in a narrow temperature range [22–25], the SmA^* → SmC^* transition was studied based on XRD patterns registered at each 0.1 °C. The determined values of the smectic layer spacing in the vicinity of the clearing temperature are shown in Fig. 6(b).

A significant difference in the temperature dependence of d at the SmA^* → SmC^* transition for $m = 5$ and $m = 6, 7$ is visible from Fig. 6. For 3F6HPhF6, a discontinuous decrease of the smectic layer spacing is observed on cooling, with the relative layer shrinkage $(d_{SmA^*} - d_{SmC^*})/d_{SmA^*}$ equal to 5%. The average layer spacing in the SmA^* phase of 3F6HPhF6 is 35.5(3) Å, which is equal to 97% of the shortest l value obtained for the *max*2 conformation, and 90% of the largest mean L value for the *max*1 + 4 set. The results for $m = 6$ resemble those for $m = 7$, which were reported previously in Ref. [22]. For $m = 7$, there is also a discontinuous shrinkage of ca. 5% in the smectic layer spacing at the SmA^* → SmC^*

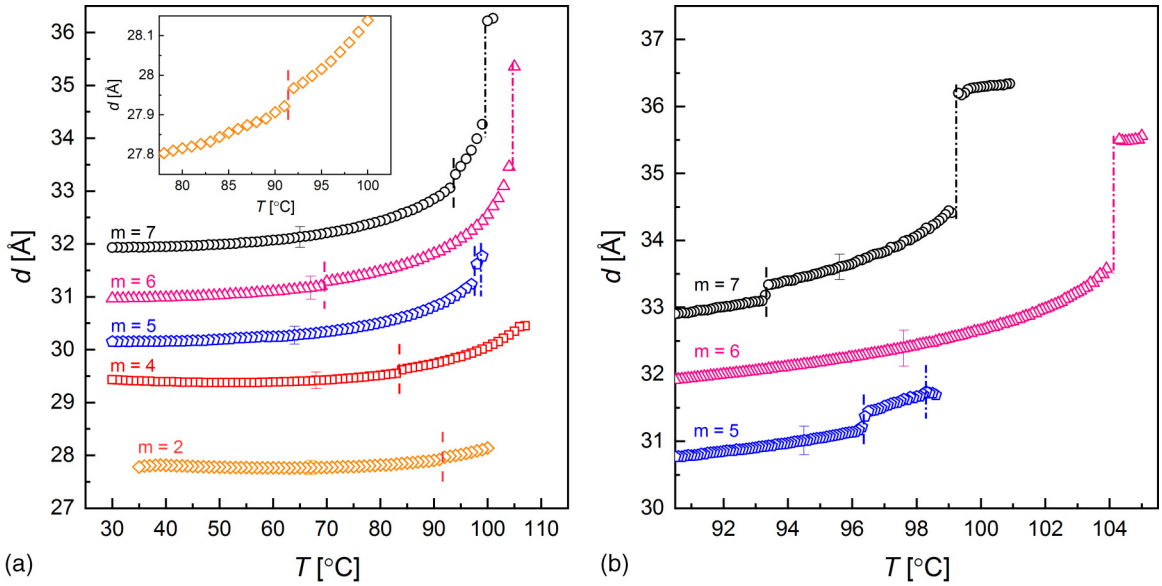

FIG. 6. Smectic layer spacing d in the 3FmHPhF6 series determined based on low-angle XRD patterns collected on cooling: in a wide temperature range (a) and in the vicinity of the phase transitions for $m = 5$, 6, 7 (b). The inset in (a) shows the results for 3F2HPhF6 about the SmC^* → SmC_A^* transition. The dashed and dash-dotted lines mark, respectively, the SmC^* → SmC_A^* and the SmA^* → SmC^* transition. For each compound, one representative uncertainty bar is shown. The layer spacing for $m = 7$ was taken from [22], after correction of the systematic error determined on the basis of the wide-angle XRD pattern.

transition, and the average $d_{\mathrm{Sm}A^*}$ value is 36.3(3) Å, which is equal to 90% of the molecular length for the *max*1 + 4 set, and even exceeds the shortest average length of the 3F7HPhF6 molecule in the *gauche*2 set ($l = 35.6$ Å). The comparison of XRD results for $m = 6$, 7 with DFT calculations implies that for these two homologues the SmA^* phase is the classical orthogonal phase with the tilt angle of particular molecules close to zero.

For 3F5HPhF6, the temperature dependence of the layer spacing is continuous at the SmA^* → SmC^* transition; however, the layer spacing slightly increases in the SmA^* phase and decreases in the SmC^* phase with decreasing temperature. The average d value in the SmA^* phase of 3F5HPhF6 is 31.7(2) Å. The shortest average molecular length, obtained by DFT calculations for the *gauche*2 set, is 33.4 Å, which corresponds to the d/l ratio = 95%; for other considered conformations the d/l ratio is 83%–90%. These results imply that for $m = 5$ the SmA^* phase is rather of the de Vries type [12,13]. In such a phase the molecules are tilted; therefore the smectic layer spacing is similar to that in the neighboring SmC^* phase and the SmA^* → SmC^* transition can occur with the negligible layer shrinkage. The tilt in the de Vries SmA^* phase has a random direction, which causes the average tilt angle to be zero. The fact that this transition occurs with almost no layer shrinkage reduces the number of so-called chevron defects in the liquid crystal alignment that would appear otherwise due to abrupt change in the layer spacing [9,12].

C. Exploration of molecular conformations

The smectic layer spacing d in the SmC^* and SmC_A^* phases, determined by XRD, and the molecular length l and shape parameter $\delta\Theta$, obtained from DFT calculations, were collectively used to calculate the tilt angle according to Eq. (1). Calculations were done by inserting Eq. (1) into Eq. (2), which means that $\langle\Theta\rangle = \langle\arccos(d/l)\rangle + \langle\delta\Theta\rangle$. For $m = 7$, the previously published d values vs temperature [22], corrected herein by the systematic shift, were used in the calculations. The uncertainties of the tilt angle $\Delta\Theta$, determined solely from the experimental uncertainty of the smectic layer spacing $\Delta d = 0.2$–0.3 Å, are equal to ca. 0.5°. When one assumes the uncertainty of 0.5 Å of the molecular length, the $\Delta\Theta$ values reach 1.5–2 Å.

The computed tilt angle vs temperature dependence for each studied 3FmHPhF6 homologue is shown in Figs. 7(a)–7(e) along with the results of the electro-optic measurements (Θ_{POM}). For easier comparison, the average tilt angle values below 50 °C (where its value is saturated) for each compound are plotted in Fig. 7(e). Although it can be seen that the tilt angle values calculated from Eq. (1) differ quantitatively for each of the considered sets of structures, all of the homologues exhibit a very similar dependence on temperature and correctly reproduce the trend shown by electro-optic measurements. It is, however, evident that the best numerical agreement between Θ_{POM} and the computed tilt angle is obtained for the *max*2 conformation and the set of the *gauche*2 structures. The average Θ_{POM} below 50 °C is equal to 43.2°–43.5° and practically does not depend on the length of the C_mH_{2m} chain [25,26], while for *max*2 and *gauche*2 the corresponding tilt angle is in the 40.6°–45.9° range. For *max*1 + 4 and *gauche*1 + 4, the tilt angle is overestimated, as the average values below 50 °C are within the 45.3°–50.2° range. The corresponding values for the *gauche*3 set are in most cases even higher, equal to 46.7°–55.1°, and only $m = 2$ *gauche*3 gives lower tilt angle values than *max*1 + 4. The most significant overestimation of the average Θ_{POM} below 50 °C is obtained for the *max*3 conformation showing the

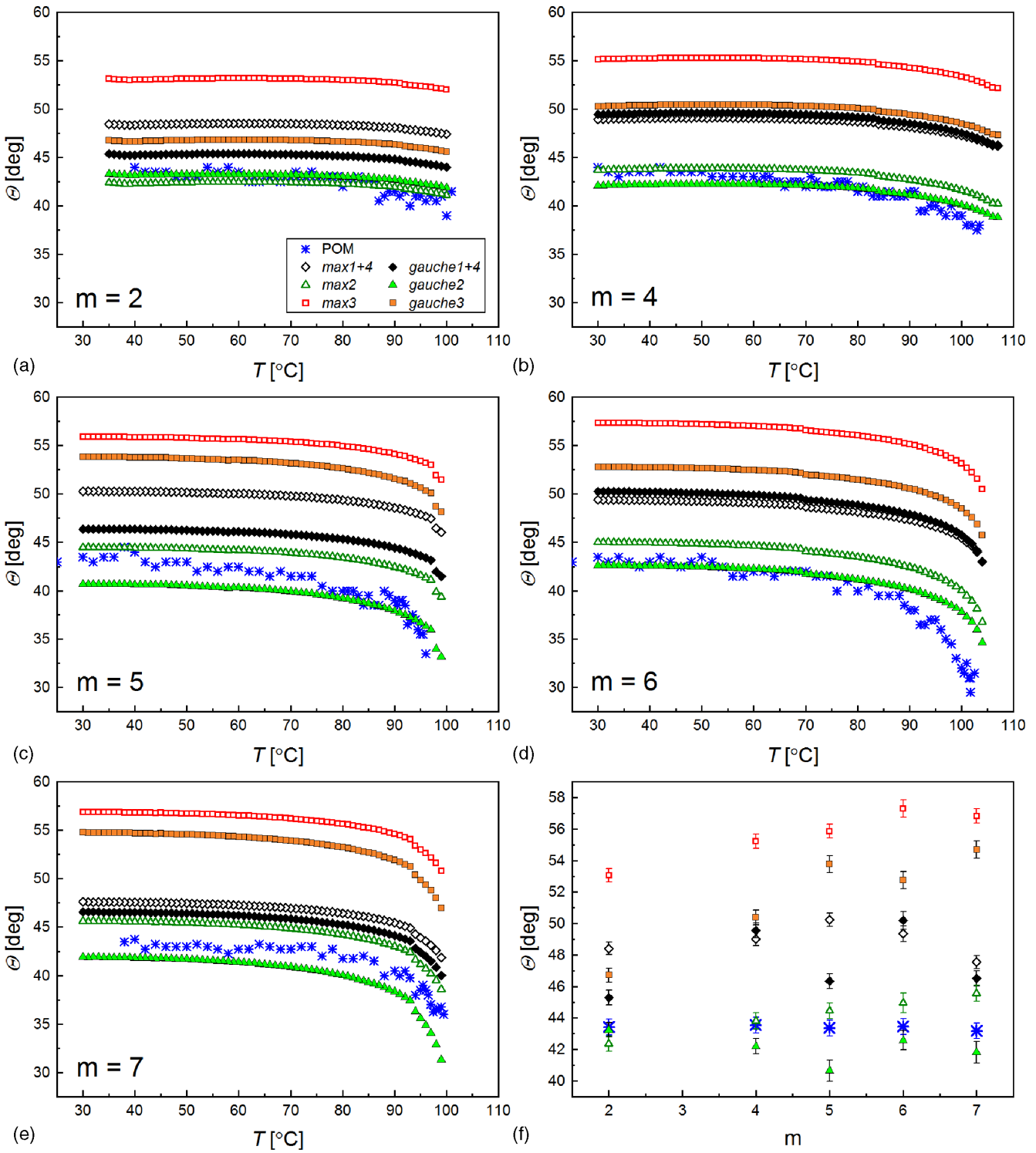

FIG. 7. Tilt angle in the SmC^* and SmC^*_A phases of 3FmHPhF6 homologues: $m = 2$ (a), $m = 4$ (b), $m = 5$ (c), $m = 6$ (d), and $m = 7$ (e) determined from the XRD and DFT results combined according to Eq. (1). The tilt angle determined by the electro-optic method [25,26] is shown for a comparison. The average tilt angle values below 50 °C for each studied homologue are presented in (f).

average tilt angle values equal to 53.1°–57.3°. In addition to the discrepancy of such high tilt angle values with the POM results, we further note that a tilt angle exceeding 45° is generally very unlikely, because it has usually been observed for V-shaped dimers, wherein the large tilt angle above 45° is imposed by the angle between two monomers [40,41]. The results in Fig. 7 therefore imply that the zigzag shape is not significantly populated in any case, and that the most probable molecular shape is the C shape, represented here by the *max*2 and *gauche*2 structures. The hockey-stick shape is also probable, as for the *gauche*1 + 4 set the overestimation of the tilt angle for $m = 2$, 5, 7 is not large (note that

the uncertainty bars presented in Fig. 7(f) include only the uncertainty of the smectic layer spacing). Furthermore, our results show that in order to use such molecule-based models in these systems it is necessary to include in the calculations *gauche*-type conformations in the longer terminal chain, as they are more energetically favorable and may demonstrate tilt angle values close to experimental measurements. Herein, we considered only two types of such conformations, but we note there are many more possible ways of "bending" the terminal chain, and this number of ways increases with the increasing length of the C_mH_{2m} chain. Especially at high temperatures, where the intermolecular distances are larger, more molecules likely adopt the *gauche* conformations. This would lead to smaller molecular lengths, which explains why the discrepancy between Θ_{POM} and the tilt angle determined using Eq. (1) usually increases with increasing temperature, especially for $m = 6$. Overall, the presented data show that the comparison of the tilt angle measured electro-optically with the tilt angle determined from the XRD results and DFT calculations can be applied to infer the most probable molecular shape within the smectic layers.

IV. SUMMARY AND CONCLUSIONS

A study was presented on chiral esters from the 3F*m*HPhF6 series ($m = 2$, 4–7), which have three phenyl rings within a rigid core and two flexible terminal carbon chains. This family of smectogens is a good example of liquid crystals that exhibit a significant discrepancy between the values of the tilt angle determined from electro-optic measurements, Θ_{POM}, and those obtained from x-ray diffraction experiments (reported as so-called steric tilt angles). DFT calculations were used here to aid in determinations of the steric tilt angle by focusing on how a molecule can deviate from a rodlike shape; this was done by modeling isolated molecules in 20 different conformations and then determining every conformation's molecular length and a shape parameter (which accounts for the relative alignment of the molecule's rigid core). It was found that different conformations come with nonequal probabilities, so Boltzmann averaging was employed. In general, the best agreement of the calculated tilt angle value with the Θ_{POM} value was obtained when a C-shape derived geometry was assumed for the molecules; this includes when the terminal carbon chain is in a fully extended conformation and when it is in the considered *gauche* conformations. The agreement is especially good below the saturation temperature (i.e., the temperature below which the tilt angle stays almost constant), which is the most important temperature region from a practical point of view. Regarding the other two considered molecular shapes, (i) the assumption of the hockey-stick shape leads to a visible overestimation of the tilt angle, although for the corresponding *gauche* models the agreement is acceptable for three homologues, and (ii) the zigzag shape of molecules is the least probable, as it reproduces the tilt angle relatively well only for the shortest homologue after an introduction of two *gauche* conformations. In summary, the method presented in this work enables a determination of the most probable conformations adopted by the molecules in the smectic phases of 3F*m*HPhF6 homologues.

The results for the homologues exhibiting the paraelectric SmA^* phase suggest that in the vicinity of the transition to this phase, the number of *gauche* conformations increases. Another conclusion is that the diversity of conformations increases with increasing temperature. At temperatures well below the clearing temperature, the intermolecular distances are smaller and, therefore, the closely packed molecules are expected to adopt a similar shape. For $m = 6$, 7 the comparison of the smectic layer spacing in the SmA^* phase with the calculated molecular length allows us to conclude that the molecules are not considerably tilted from the layer normal. This indicates a standard orthogonal smectic phase. For $m = 5$, the obtained d/l ratio of 83%–95% and the lack of discontinuity in the observed layer spacings during the Sm$A^* \rightarrow$ SmC^* transition prove that the SmA^* phase of this homologue is of the de Vries type and the Sm$A^* \rightarrow$ SmC^* transition can be described as a disorder-order transition of the tilt direction.

In conclusion, x-ray diffraction studies combined with adequate quantum-mechanical calculations are shown to be a useful tool to study the structure and arrangement of molecules in the smectic phases, as long as different conformations of the molecules are taken into account and, in the case of the tilted smectic phases, a comparison with the results of the complementary electro-optic method is possible.

ACKNOWLEDGMENTS

We would like to thank Professor Damian Pociecha (Faculty of Chemistry, University of Warsaw) for x-ray diffraction measurements and Professor Wojciech Zając (Institute of Nuclear Physics Polish Academy of Sciences) for discussions regarding the molecular modeling. The PL-Grid Infrastructure and the Academic Computer Centre Cyfronet AGH, Kraków, Poland (Grants No. plgmolkryst, No. molkryst7, and No. soliddft2020) are gratefully acknowledged for providing computational resources. Financial support from the Ministry of Science and Higher Education in Poland ("Outstanding Young Scientist" scholarship to J.H.) is gratefully acknowledged. This research was supported in part by the Excellence Initiative Research University Program at the Jagiellonian University in Kraków.

The authors report no potential conflict of interest.

[1] G. Vertogen and W. H. de Jeu, *Thermotropic Liquid Crystals, Fundamentals* (Springer, Berlin, 1988).

[2] P. Rudquist, in *Handbook of Visual Display Technology*, edited by J. Chen, W. Cranton, and M. Fihn (Springer, Berlin, 2012).

[3] J. P. F. Lagerwall and F. Giesselmann, ChemPhysChem **7**, 20 (2006).

[4] J. P. F. Lagerwall and G. Scalia, Curr. Appl. Phys. **12**, 1387 (2012).

[5] J. Wu, T. Usui, and J. Hanna, J. Mater. Chem. **21**, 8045 (2011).

[6] R. Teerakapibal, C. Huang, A. Gujral, M. D. Ediger, and L. Yu, Phys. Rev. Lett. **120**, 055502 (2018).

[7] N. A. Clark and S. T. Lagerwall, Appl. Phys. Lett. **36**, 899 (1980).

[8] A. D. L. Chandani, Y. Ouchi, H. Takezoe, A. Fukuda, K. Terashima, K. Furukawa, and A. Kishi, Jpn. J. Appl. Phys. **28**, L1261 (1989).

[9] K. D'have, P. Rudquist, S. T. Lagerwall, H. Pauwels, W. Drzewiński, and R. Dąbrowski, Appl. Phys. Lett. **76**, 3528 (2000).

[10] J. T. Mills, H. F. Gleeson, J. W. Goodby, M. Hird, A. Seed, and P. Styring, J. Mater. Chem. **8**, 2385 (1998).

[11] H. F. Gleeson, Y. Wang, S. Watson, D. Sahagun-Sanchez, J. W. Goodby, M. Hird, A. Petrenko, and M. A. Osipov, J. Mater. Chem. **14**, 1480 (2004).

[12] J. P. F. Lagerwall, F. Giesselmann, and M. D. Radcliffe, Phys. Rev. E **66**, 031703 (2002).

[13] A. De Vries, A. Ekachai, and N. Spielberg, Mol. Cryst. Liq. Cryst. **49**, 143 (1979).

[14] P. Morawiak, M. Żurowska, and W. Piecek, Liq. Cryst. **45**, 1451 (2018).

[15] W. Piecek, Z. Raszewski, P. Perkowski, J. Kędzierski, J. Rutkowska, J. Zieliński, E. Nowinowski-Kruszelnicki, R. Dąbrowski, M. Tykarska, and J. Przedmojski, Mol. Cryst. Liq. Cryst. **436**, 149 (2005).

[16] W. Piecek, Z. Raszewski, P. Perkowski, J. Przedmojski, J. Kędzierski, W. Drzewiński, R. Dąbrowski, and J. Zieliński, Ferroelectrics **310**, 125 (2004).

[17] V. Novotná, V. Hamplová, A. Bubnov, M. Kašpar, M. Glogarová, N. Kapernaum, S. Bezner, and F. Giesselmann, J. Mater. Chem. **19**, 3992 (2009).

[18] A. Bubnov, M. Kašpar, V. Novotná, V. Hamplová, M. Glogarová, N. Kapernaum, and F. Giesselmann, Liq. Cryst. **35**, 1329 (2008).

[19] N. Podoliak, V. Novotná, M. Glogarová, V. Hamplová, M. Kašpar, A. Bubnov, N. Kapernaum, and F. Giesselmann, Phase Trans. **83**, 1026 (2010).

[20] D. Ziobro, R. Dąbrowski, M. Tykarska, W. Drzewiński, M. Filipowicz, W. Rejmer, K. Kuśmierek, P. Morawiak, and W. Piecek, Liq. Cryst. **39**, 1011 (2012).

[21] S. M. Said, Yu. Semenova, Y. P. Panarin, A. Bubnov, M. Glogarová, M. Kašpar, and V. Hamplová, Ferroelectrics **311**, 11 (2004).

[22] A. Deptuch, T. Jaworska-Gołąb, M. Marzec, D. Pociecha, J. Fitas, M. Żurowska, M. Tykarska, and J. Hooper, Phase Trans. **91**, 186 (2018).

[23] M. Żurowska, R. Dąbrowski, J. Dziaduszek, K. Czupryński, K. Skrzypek, and M. Filipowicz, Mol. Cryst. Liq. Cryst. **495**, 145 (2008).

[24] M. Żurowska, R. Dąbrowski, J. Dziaduszek, K. Garbat, M. Filipowicz, M. Tykarska, W. Rejmer, K. Czupryński, A. Spadło, N. Bennis, and J. M. Otón, J. Mater. Chem. **21**, 2144 (2011).

[25] A. Deptuch, M. Marzec, T. Jaworska-Gołąb, M. Dziurka, J. Hooper, M. Srebro-Hooper, P. Fryń, J. Fitas, M. Urbańska, and M. Tykarska, Liq. Cryst. **46**, 2201 (2019).

[26] A. Deptuch, A. Drzewicz, M. Dziurka, N. Górska, J. Hooper, T. Jaworska-Gołąb, E. Juszyńska-Gałązka, M. Marzec, M. Piwowarczyk, M. Srebro-Hooper, M. Tykarska, and M. Urbańska, Mater. Res. Bull. **150**, 111756 (2022).

[27] A. Deptuch, S. Lalik, M. Jasiurkowska-Delaporte, E. Juszyńska-Gałązka, A. Drzewicz, M. Urbańska, and M. Marzec, Phys. Rev. E **105**, 024705 (2022).

[28] M. J. S. Dewar, E. G. Zoebisch, E. F. Healy, and J. J. P. Stewart, J. Am. Chem. Soc. **107**, 3902 (1985).

[29] M. J. Frisch, G. W. Trucks, H. B. Schlegel, G. E. Scuseria, M. A. Robb, J. R. Cheeseman, G. Scalmani, V. Barone, G. A. Petersson, H. Nakatsuji, X. Li, M. Caricato, A. V. Marenich, J. Bloino, B. G. Janesko, R. Gomperts, B. Mennucci, H. P. Hratchian, J. V. Ortiz, A. F. Izmaylov *et al.*, GAUSSIAN09, Revision D.01 (Gaussian, Inc., Wallingford, CT, 2013).

[30] J. J. P. Stewart, J. Mol. Model. **19**, 1 (2013).

[31] J. J. P. Stewart, *MOPAC2016* (Stewart Computational Chemistry, Colorado Springs, CO, 2016).

[32] A. D. Becke, Phys. Rev. A **38**, 3098 (1988).

[33] C. Lee, W. Yang, and R. G. Parr, Phys. Rev. B **37**, 785 (1988).

[34] S. Grimme, S. Ehrlich, and L. Goerigk, J. Comput. Chem. **32**, 1456 (2011).

[35] A. Schäfer, H. Horn, and R. Ahlrichs, J. Chem. Phys. **97**, 2571 (1992).

[36] K. Eichkorn, F. Weigend, O. Treutler, and R. Ahlrichs, Theor. Chem. Acc. **97**, 119 (1997).

[37] F. Weigend and R. Ahlrichs, Phys. Chem. Chem. Phys. **7**, 3297 (2005).

[38] M. D. Hanwell, D. E. Curtis, D. C. Lonie, T. Vandermeersch, E. Zurek, and G. R. Hutchison, J. Cheminf. **4**, 17 (2012).

[39] Y. Yamamura, T. Murakoshi, M. Hishida, and K. Saito, Phys. Chem. Chem. Phys. **19**, 25518 (2017).

[40] N. Olsson, I. Dahl, B. Helgee, and L. Komitov, Liq. Cryst. **31**, 1555 (2004).

[41] N. Olsson, M. Schröder, S. Diele, G. Andersson, I. Dahl, B. Helgee, and L. Komitov, J. Mater. Chem. **17**, 2517 (2007).